Phase-field modeling of an immiscible liquid-liquid displacement in a capillary

S. Prokopev,[1] A. Vorobev,[2,*] and T. Lyubimova[1,3]

[1]*Institute of Continuous Media Mechanics UB RAS, Perm 614013, Russia*

[2]*Faculty of Engineering and Physical Sciences, University of Southampton, Southampton SO17 1BJ, United Kingdom*

[3]*Perm State University, Perm 614990, Russia*

(Received 15 January 2019; published 21 March 2019)

We develop a numerical model for a two-phase flow of a pair of immiscible liquids within a capillary tube. We assume that a capillary is initially saturated with one liquid and the other liquid is injected via one of the capillary's ends. The governing equations are solved in the velocity-pressure formulation, so the pressure levels are imposed at the capillary inlet and outlet ends. We model the structure of the flow and the shape of the interface. We are able to reproduce the flow for a wide range of capillary numbers, when the meniscus preserves its shape moving together with the flow, and when the meniscus constantly stretches resembling the transport of a passive impurity. We demonstrate that the phase-field approach is capable of reproducing all features of the liquid-liquid displacement, including the motion of a contact line, the dynamic changes of the capillary pressure, and the dynamic changes of the apparent contact angle.

DOI: 10.1103/PhysRevE.99.033113

I. INTRODUCTION

We aim to develop a theoretical model for description of a liquid-liquid displacement in a porous medium. We assume that the porous medium is initially saturated with one liquid that is displaced by injection of another liquid. Numerous processes in nature and industry can be reduced to a similar physical configuration, including oil recovery and aquifer and soil remediation.

A macroscopic description of a liquid-liquid displacement in a porous medium is traditionally given in the framework of an extended Darcy model that is adopted for multiphase flows. The model introduces such phenomenological parameters as the relative permeabilities and the capillary pressure that strongly depend on the relative amounts of liquids in a porous matrix, which essentially means that the theory incorporates not three but a (infinite) number of phenomenological constants, as the experimental determination of the functions (or curves) of the relative permeabilities and capillary pressure requires a series of measurements of these quantities for a number of saturation levels. This fact renders the numerical results obtained on the basis of the Darcy model less valuable, making the results site and fluids specific.

For a more universal understanding of multiphase flows through a porous medium a pore-level analysis is required. A pore-level model is usually based on the network approach when the porous matrix is represented as a network of interconnected capillaries, that, for a more general representation, may be taken with different (random) diameters [1,2]. Hence, for understanding of a multiphase flow in a porous medium, the initial task is reduced to the accurate description of a multiphase flow within a single capillary, which is undertaken in the current work.

The first studies of multiphase flows in a capillary were carried out by West [3] and Washburn [4]. It was established that for low Reynolds and capillary numbers (that are defined as $\mathrm{Re} = \rho_* V_* d/\eta_*$ and $\mathrm{Ca} = V_* \eta_*/\sigma_*$, where V_* is the typical velocity of the flow in a capillary, d is the capillary's diameter, ρ_* is the typical density, η_* is the viscosity coefficient, and σ_* is the surface tension coefficient), the flow structure has a parabolic Poiseuille profile, with an axisymmetric meniscus that moves with the same speed as the rest of the liquids (like a piston that displaces one of the liquids). The speed of the flow is determined by the pressure difference that is reduced by the value of the capillary pressure associated with the curved interface. It was later pointed out that the capillary pressure, associated with the liquid-liquid meniscus, is to be given by an apparent contact angle that is different from the static contact angle and that is determined by the flow rate [5].

In the cases of stronger injections, when the flow rates and hence the capillary numbers are higher, the displacement of one liquid by another occurs differently. A meniscus in this case has a finger-type shape, with the injected fluid penetrating through the middle section of the capillary, displacing the liquid at the far end, and leaving some liquid on the capillary's wall. This is termed a fingering displacement. The major focus is to investigate the ratio of the volume of the displaced liquid over the volume that remains deposited on the capillary's walls as a function of the capillary number [6]. The theoretical modeling of a fingering displacement was undertaken by Cox [7], who developed an approximate theory capable of predicting the flow pattern near the liquid-liquid interface, and the value of the fraction left on the tube's walls. The most recent series of works was probably published by Soares *et al.* [8–10], who developed the Galerkin finite element numerical technique for the modeling of a liquid-liquid flow in a capillary.

These studies were also extended onto consideration of the displacement of the liquid by another liquid when the

*A.Vorobev@soton.ac.uk

liquids are miscible [11,12]. The miscible liquids correspond to a limiting case of the fingering displacement, when the capillary number is (infinitely) large due to low (absent) interfacial stresses. For miscible liquids, a new parameter, the Peclet number ($\mathrm{Pe} = V_* d/D_*$, where D_* is the diffusion coefficient), needs to be introduced. It is found that for larger values of the Peclet numbers (above $\mathrm{Pe} \sim 1000$) the observed behavior agrees with immiscible systems (for the case of large capillary numbers), with a clearly visible sharp interface that separates the fluids and even the values of the surface tension coefficient for this miscible interface could be estimated ($\sim$0.43 dyn/cm). For lower Peclet numbers the experimental results were difficult to obtain due to strong smearing of interfaces.

The numerical model for miscible systems was developed by Chen and Meiburg [12], who represented a pair of miscible liquids as a homogeneous system (as a single-phase fluid with impurity, neglecting capillary effects). The results of Chen and Meiburg [12] agree with the experimental observations achieved for the case of higher Peclet numbers.

The current paper provides the results of the direct numerical simulation of an immiscible liquid-liquid displacement. The numerical model is built up on the basis of the phase-field approach, that introduces the possibility of mixing between two phases. Nevertheless, in the current work, we always assume that diffusive transport is negligible at least for the duration of the displacement run and hence the liquids remain immiscible. The advantages of the phase-field approach are the ability of tracing the changes of the interface shape and the ability of modeling the capillary and wetting properties (including the modeling of the contact line slippage) that determine the overall dynamics of a liquid-liquid displacement.

II. PROBLEM STATEMENT

A. Phase-field model: Governing equations

Within the phase-field approach the system of two liquids is represented as a heterogeneous binary mixture. The position of an interface is traced through the field of concentration, that is defined as the mass fraction of one of the liquids in a liquid-liquid mixture. A single set of the governing equations is written for the entire multiphase system, including the interface boundary, that is represented as a transitional layer of a finite thickness (across the boundary all variables experience sharp but continuous changes). To take into account the surface tension effects existent at interfaces, the free energy function of a mixture is redefined as follows [13]:

$$f = f_0(C) + \frac{\epsilon}{2}(\nabla C)^2. \tag{1}$$

Here f is the total specific free energy function and f_0 is its classical part. The magnitude of the additional term is given by the capillary constant ϵ, that is assumed to be so small that this term is negligible everywhere except for the location of very strong concentration gradients that correspond to interfaces.

The full equations that determine the evolution of a heterogeneous binary mixture with the states given by the free energy function (1) are called the Cahn-Hilliard-Navier-Stokes equations [14]. The full equations are rather difficult for numerical treatment, with the main difficulty caused by the effect of quasicompressibility (the continuity equation needs to be used in the full form owing to dependence of the mixture density on concentration). In all works (e.g., Refs. [15–17]), the numerical solution is given in the framework of the Boussinesq approximation of the full equations. The Boussinesq approximation of the Cahn-Hilliard-Navier-Stokes equations was strictly derived in paper [18], and this approximation is employed in the current work.

The governing equations include the laws of conservation for momentum, species, and mass:

$$\frac{\partial \vec{u}}{\partial t} + (\vec{u}\cdot\nabla)\vec{u} = -\nabla\Pi + \frac{1}{\mathrm{Re}}\Delta\vec{u} - \frac{1}{M}C\nabla\mu, \tag{2}$$

$$\frac{\partial C}{\partial t} + (\vec{u}\cdot\nabla)C = \frac{1}{\mathrm{Pe}}\Delta\mu, \tag{3}$$

$$\nabla\cdot\vec{u} = 0. \tag{4}$$

Here t is the time and $\vec{u}$ is the velocity vector (velocity is defined as the mass-averaged velocity of a fluid particle that includes two components of a mixture). The quantity Π stands for the modified pressure that needs to be determined through the incompressibility constraint. The real pressure is given by the following expression:

$$p = \Pi - \frac{1}{M}\left(\mathrm{Cn}\frac{(\nabla C)^2}{2} - \mu C + f_0\right). \tag{5}$$

One sees that the right-hand side of Eq. (2) includes an additional term that is frequently called the Korteweg force. This term determines the action of the capillary forces that define the shape of the interfacial boundary. In the equation for the species balance (3) the diffusion term is given by using the generalized Fick's law, that defines the diffusion flux proportional to the gradient of the chemical potential. The chemical potential μ is set by the expression

$$\mu = \frac{df_0}{dC} - \mathrm{Cn}\Delta C. \tag{6}$$

The equations are written in the nondimensional form. The quantities h, $V_{\max}$, $h/V_{\max}$, $\rho_* V_{\max}^2$, μ_* that set a typical flow in a capillary are chosen as the scales of length, velocity, time, pressure, and chemical potential. Here h is the diameter of a tube, $V_{\max}$ is the maximum velocity, and μ_* and ρ_* are the typical values of the chemical potential and density.

The governing equations include the Reynolds, Peclet, Mach, and Cahn numbers,

$$\mathrm{Re} = \frac{\rho_* V_{\max} h}{\eta_*}, \quad \mathrm{Pe} = \frac{\rho_* V_{\max} h}{\alpha_* \mu_*},$$
$$M = \frac{V_{\max}^2}{\mu_*}, \quad \mathrm{Cn} = \frac{\epsilon}{\mu_* h^2}. \tag{7}$$

The Reynolds number defines the ratio between the inertia and viscous forces. For flows in a capillary the primary interest plays the limit of low Reynolds numbers when the inertia terms are negligible (although, in some porous media, e.g., in fixed beds of chemical reactors, the Reynolds numbers may be as high as 1000 [19]). The Peclet number determines the role of diffusion effects. Considerable smearing of an initially sharp interface should occur after a time period of

the order ∼Pe. In the current study we focus on the dynamics of immiscible displacement, and we assume that Pe $\gg 1$ and that the time needed for a liquid-liquid meniscus to move through the whole tube is also much smaller than Pe. The Mach number determines the role of the capillary effects in the Navier-Stokes equation. The Cahn number determines the thickness of the liquid-liquid interface, as $\delta = \sqrt{2\mathrm{Cn}}$ [14,18].

It should be added that the set of Eqs. (2)–(4) assumes that two liquids of a mixture are characterized by similar viscosity coefficients. For derivation of these equations [18], it was assumed that the viscosity coefficients of the liquids are different, although the difference is small, so the leading term of the viscous force, that is kept in the equations, includes just one single parameter, that may be defined as the average viscosity of two liquids.

Finally, we need to define the expression for the classical free energy function f_0 that determines the equilibrium states of a binary mixture (with omission of capillary effects) [20]. We are interested in the dynamics of a pair of immiscible liquids. Such a mixture can be effectively represented by the so-called double-well potential (see, e.g., Refs. [15–17]), that can be written as

$$f_0 = -\tfrac{1}{2}C^2 + C^4. \tag{8}$$

This expression has two minima, $C = \pm\frac{1}{2}$, that correspond to two pure components of the binary mixture.

B. Geometry: Boundary conditions

The governing equations are solved for a capillary that is represented by a plane layer with two plates of length L separated by a unit distance. The results shown below are obtained for the layers of the length $L = 6$. This length was found to be long enough for a sufficiently long evolution of the liquid-liquid interface that would allow for general conclusions to be made. The numerical runs were also conducted for longer tubes, with $L = 12$, and no significant differences were observed. The consideration in the current work is restricted to the two-dimensional (2D) problem, with the Cartesian coordinates, x and y, along and across the layer.

For the initial state we assume that the layer is filled with two liquids, so that the first liquid occupies a small region at the left end of the tube, and the second liquid occupies the rest of the tube. Thus the initial concentration profile is determined by the expression

$$C_0 = \frac{1}{2}\tanh\left(\frac{x - x_0}{\delta_0}\right). \tag{9}$$

Here x_0 is the initial position of the liquid boundary (usually, $x_0 = 0.5$). Initially the liquids are stationary and they are separated by a thin flat vertical interface of a thickness $\delta_0 = \sqrt{2\mathrm{Cn}}$. At the initial time moment, the fluids stay at rest ($\vec{u} = 0$). The flow is driven by the pressure gradient enforced between the ends of a capillary that is switched on at the time moment $t = 0$. The effect of gravity is neglected: we assume that the hydrostatic pressure is negligibly small as compared with the capillary pressure and the pressure difference imposed between the tube ends (e.g., due to a lower density contrast).

The governing equations are supplemented by the following boundary conditions, at the upper and lower plates:

$$y = 0, 1: \; u_x = u_y = 0, \quad \frac{\partial \mu}{\partial y} = 0, \quad \frac{\partial C}{\partial y} = 0; \tag{10}$$

at the left end of a capillary,

$$x = 0: \; p = p_1, \quad \frac{\partial \mu}{\partial x} = 0, \quad \frac{\partial C}{\partial x} = 0; \tag{11}$$

and at the right end,

$$x = L: \; p = 0, \quad \frac{\partial \mu}{\partial x} = 0, \quad \frac{\partial C}{\partial x} = 0. \tag{12}$$

Thus at the rigid plates we impose the standard no-slip boundary condition for the velocity and the absence of the diffusion flux (that is set by the gradient of the chemical potential) through the boundary. The additional condition for the concentration field sets the wetting conditions. In the current work we assume the simplest case of the wetting condition when the molecules of the walls interact with the molecules of two liquids equally, so the contact line is orthogonal to the wall. At the inlet and outlet boundaries we set the pressure levels. We also impose the zero normal derivatives of the chemical potential and concentration assuming continuity of matter at the capillary's ends.

The reference point for the pressure field is set at the right (outlet) end of the tube. The pressure level at the left (inlet) end of the tube is always set as

$$p_1 = \frac{8L}{\mathrm{Re}}. \tag{13}$$

This value is chosen so that the maximum value of the velocity (the velocity at the centreline) is equal to 1 for a single-phase flow. Thus, in the simulations shown below, the pressure gradient along the tube depends on the Reynolds number. For the single-phase flow (negligible capillary effects) the velocity profile always remains the same,

$$u_x = 4y(1 - y); \; u_y = 0, \tag{14}$$

independent on the flow parameters.

C. Modeling of a contact line

A difficulty of the modeling of two-phase flows through a capillary is given by a necessity to describe the motion of a contact line [21]. Indeed, along the wall, the no-slip condition is imposed for the fluid velocity (10), which seems not to conform with the motion of the contact line that can be observed in numerous experiments. To resolve this difficulty, traditional sharp-interface models adopt a different condition for the velocity field along the wall,

$$\left(u_x + L_s\frac{\partial u_x}{\partial y}\right)_{\mathrm{wall}} = 0, \tag{15}$$

that introduces an additional phenomenological parameter L_s, called the slip length. Although, as was shown by Jacqmin [22], within the phase-field simulations the motion of a contact line can be naturally obtained from the solution of the governing Eqs. (2)–(4), and the use of the additional slip model is not needed. To achieve this conclusion Jacqmin conducted the work along two supplementary paths.

Jacqmin fulfilled nanoscale computations of a multiphase flow with the use of realistic liquid-liquid diffusivities and with the use of the model for the shear-induced slip (15). He demonstrated that with the no-slip condition "diffusion can maintain the interface profile" for diffusivities as small as $D_* \sim 10^{-11}$ m^2 s^{-1}. At $D_* \sim 10^{-12}$ m^2 s^{-1} "the contact line is maintained but the interface profile is distorted," and at $D_* \sim 10^{-13}$ m^2 s^{-1} "the contact line begins to fail." Next, he showed that if $D_* \sim 10^{-10}$ m^2 s^{-1} and slip length $L_s = 10^{-8}$ m, then slip effects are dominant. For the same diffusivity, but $L_s = 10^{-9}$ m, "slip and diffusion are competitive in effect. With $L = 10^{-10}$ m diffusion effects are dominant." He also noticed that the molecular level simulations indicate slip lengths of at most about $L_s = 3 \times 10^{-10}$ m, and thus, for realistic slip lengths, diffusion effects are dominant over shear-induced slip.

Jacqmin also examined the asymptotic behavior of flow fields inside and outside the contact line region, which allowed him to draw that "to leading order the outer-region velocity field is the same as for sharp interfaces while the chemical potential behaves like $\ln(r)/r$" (when the equilibrium contact angle $\alpha_{eq} = 90^\circ$). "The diffusive and viscous contact line singularities implied by these outer solutions are resolved in the inner region through chemical diffusion. The length scale of the inner diffusion is about $10\sqrt{\eta_*\alpha_*}/\rho_*$. Diffusive fluxes in this region are $O(1)$. These counterbalance the effects of the velocity, which, because of the assumed no-slip boundary condition fluxes material through the interface in a narrow boundary layer next to the wall."

On the basis of his analysis, Jacqmin concluded that the phase-field "contact line has the same far-field behavior as the more traditional sharp-interface slip models of contact line flow. A computational fluid dynamicist interested in only macroscopic results can thus use either model. Certain difficult to know parameters enter into both: in the case of slip models it is the material dependent slip-length, in the case of the phase-field model it is the material-dependent mobility."

In our work, we solely rely on the description of the contact line that is provided by the diffusion-interface approach. The motion of the contact line is then determined by the mobility coefficient α_* (or, in nondimensional formulation, by the Peclet number). Since we do not provide any empirical matching to experiments, our results remain qualitative, nevertheless, we perform simulations for different Peclet numbers, in the range from $\mathrm{Pe} = 10^3$ to $\mathrm{Pe} = 10^5$, and observe that numerical results remain qualitatively similar.

D. Estimations: Typical values of governing parameters

The full problem (2)–(4) is determined by four governing parameters (7). In addition, the capillary number that determines the ratio between the viscous and surface tension forces, is frequently used for classification of capillary flows. In terms of the already introduced parameters, the capillary number is defined as

$$\mathrm{Ca} = \frac{M}{\mathrm{Re}} = \frac{V_{\max}\eta_*}{\rho_*\mu_* h}. \tag{16}$$

The difficulty of the phase-field approach is the use of the nonstandard phenomenological coefficients, which values are not directly measurable. In particular, definitions of the nondimensional parameters (7) involve the typical value of the chemical potential μ_*, the capillary constant ϵ, and the mobility coefficient α_*.

The most important parameter, whose value is required for practical calculations, is the typical value of the chemical potential μ_*. By comparison of the phase-field definition of the capillary number (16) with its classical definition ($V_*\eta_*/\sigma_*$), one may understand that the typical value of the chemical potential may be estimated through the surface tension coefficient,

$$\mu_* = \frac{\sigma_*}{\rho_* h}. \tag{17}$$

For instance, if one assumes that $\sigma_* \sim 10^{-2}$ N/m, $\rho_* \sim 10^3$ kg/m, and $h \sim 10^{-4}$ m, then the typical value of the chemical potential may be estimated as $\mu_* \sim 0.1$ J kg^{-1}.

Next, the speed of the fluid flow in a capillary can be estimated by using the following equation:

$$V_{\max} = \frac{\Delta p}{L}\frac{h^2}{8\eta_*}. \tag{18}$$

For oil recovery applications, a typical pressure difference can be estimated as $\Delta p/L = 10^7$ Pa/10^3 m–10^4 Pa/m. We also assume that the mixture that saturates a capillary has the viscosity coefficient $\eta_* \sim 10^{-3}$ Pa s. For a capillary of the diameter $h \sim 10^{-4}$ m, the velocity of the mixture is $V_{\max} \sim 10^{-2}$m/s. In this case, the Reynolds and Mach numbers can be estimated as $\mathrm{Re} \sim 1$ and $M \sim 10^{-3}$, respectively. The capillary number is then $\mathrm{Ca} \sim 10^{-3}$.

It should be mentioned that the above estimates strongly depend on the diameter of the capillary, and for narrower capillaries the Reynolds and Mach numbers can have lower values. In addition, under subsurface conditions, both water and oil absorb gases, which lowers the value of the surface tension coefficient. The absorption rates primarily depend on pressure (on the reservoir depth), and the surface tension coefficient of the oil-water interface might be as low as 10^{-3} N/m. In this case the estimate of the Reynolds number remains unchanged, while the Mach number (and the capillary number) may be lower.

The capillary constant ϵ primarily determines the thickness of the liquid-liquid interface. In reality the interface thickness is just several molecular layers, which is zero for the macroscopic approach. This signifies that the capillary constant should be also very small. For the sake of numerical solution, the interface is represented by a transitional layer of finite thickness, and hence higher values of the capillary constant are considered. Although, to prove the physical meaning of the results, it is important to show that the numerical results converge upon gradual reduction of the capillary constant (or the Cahn number), which is done in Sec. III.

At last, we need to discuss the values of the mobility coefficient α_*. This parameter is proportional to the coefficient of diffusion D_*, and thus its value can be estimated as $\alpha_* = \rho_* D_*/\mu_*$.

We are interested in propagation of immiscible interfaces, assuming that the Peclet number is so high that diffusive processes remain insignificant. Indeed, the typical diffusive time scale is $\tau_d = Pe$, and hydrodynamic changes are determined

by a different time scale, $\tau_h = \mathrm{Re}$. Our results are obtained for $\mathrm{Pe} = 10^4$ and $\mathrm{Re} \leqslant 1$. Propagation of a meniscus through the full length of a capillary (with the length of $L = 6$) takes less than ten units of nondimensional time. Diffusion obviously does not play a significant effect over such a short time period.

On the other hand, as shown by Jacqmin [22], the mobility coefficient determines the motion of a contact line, and thus our results remain sensitive to its value, even when its values are very small (and hence when the Peclet number is very large). Most of our results are obtained for $\mathrm{Pe} = 10^4$, that would correspond to the mobility coefficient, $\alpha_* \sim 10^{-6}\ \mathrm{kg^2\,J^{-1}\,s^{-1}\,m^{-1}}$, and to the liquid-liquid diffusivity, $D_* \sim 10^{-10}\ \mathrm{m^2\,s^{-1}}$. Jacqmin [22] showed that for such diffusivities, diffusion could successfully support the motion of a contact line. The change of the actual value of the Peclet number does affect characteristics of the multiphase fluid flow, although we observe no qualitative changes in the results when the Peclet number varies in the range of 10^3 and 10^5.

III. NUMERICAL SOLUTION

The governing equations are solved numerically using the formulation of primitive variables, pressure velocity, and using the fractional-step (or projection) method that is implemented on the basis of the finite difference approach [23,24].

The numerical results are reported in the terms of the flow fields (the fields of concentration, pressure, velocity, and chemical potential), and in the terms of the integral parameters, the speed of the meniscus' tip, and contact line, the flow fluxes at the inlet or outlet, the length of the interface, the surface tension coefficient, the capillary pressure, and the apparent contact angle.

The position of the interface is determined by the concentration level, $C = 0$. To determine the speed of the meniscus' tip V_{tip} and the speed of the meniscus' ends V_{wall}, we determine the rates of changes of the corresponding points of the interface, x_{tip} and x_{wall}. To determine the length of the interface L_δ, we first search for the nodes between which the concentration changes sign and determine the position of the interface between these nodes by using the linear interpolation; we next obtain the length of an interface element that lies within the cell formed of four nodes; and finally we sum up these elementary lengths to obtain the length of the whole interface line.

To determine the apparent contact angle α, we calculate the angle between the horizontal line and the line that connects the end of the meniscus on the wall with another point on the meniscus. The x position of another point is taken as a fraction of the distance $(x_{\mathrm{tip}} - x_{\mathrm{wall}})$. Three different fractions are used, 0.25, 0.33, and 0.5, and the results are shown if the so-obtained three angles are sufficiently close to each other.

We also calculate the coefficient of the surface tension as

$$\sigma = \frac{\mathrm{Cn}}{L_\delta} \int_V \left[\left(\frac{\partial C}{\partial x} \right)^2 + \left(\frac{\partial C}{\partial y} \right)^2 \right] dV. \tag{19}$$

Here V is the volume (for the 2D case, the area) of the computational domain.

Other studies on the liquid-liquid displacement in capillaries are frequently focused on the determination of the fraction of the liquid that initially saturates a capillary, and that is left in the capillary at the end of displacement. We calculate this fraction using the definition that is based on the velocity profile [12],

$$m = 1 - \frac{Q}{V_{\mathrm{tip}}}. \tag{20}$$

Here Q is the volumetric flow flux through a capillary that is determined at the capillary's inlet or outlet (as both liquids are incompressible these two quantities are equal),

$$Q = \int_y (u_x)_{x=0,L} dy. \tag{21}$$

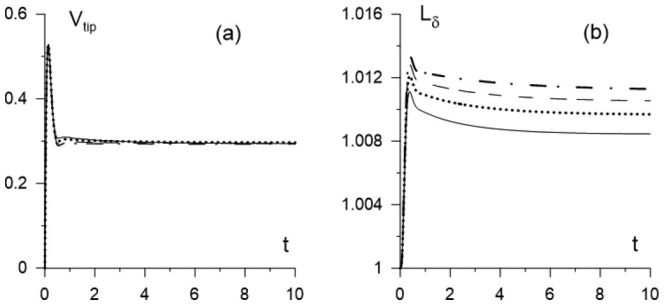

FIG. 1. (a) The velocity of the tip of the liquid-liquid meniscus and (b) the length of the meniscus vs time. The data are obtained for $\mathrm{Pe} = 10^4$, $\mathrm{Cn} = 4 \times 10^{-4}$, $\mathrm{Re} = 1$, $M = 10^{-4}$ using the numerical grids with the grid size of 1/250 (solid lines), 1/300 (dotted lines), 1/350 (dashed lines), and 1/400 (dash-dotted lines).

For validation of our numerical code, we first observed establishment of the classical Poiseuille profile (14), that is realized for sufficiently large values of Mach number (in fact, for $M = 1$) when the capillary effects become insignificant. Next, we checked the numerical convergence of our results. We found that the calculations are more challenging (exhibit slower convergence upon improvement of the numerical resolution) for lower Mach numbers ($M = 10^{-3}$ and lower). Figure 1 shows the curves obtained for $M = 10^{-4}$ for four different sizes of the grid cells. One can notice that the curves that are obtained by using the different numerical grids differ, although slightly, and upon gradual increase of the resolution, the convergence to a limiting result is observed. Based on these test runs we concluded that the resolution with the size of grid cells of 1/300 is sufficient for generation of sufficiently accurate results. Figure 2 depicts the curves obtained for different Cahn numbers (different interface thicknesses). Convergence of our results to the behavior of a two-phase system with a sharp interface can be observed, in the sense that the distance between the curves decreases when the interface thickness is taken smaller and smaller. Further, we show the results of numerical simulations for the Cahn number, $\mathrm{Cn} = 4 \times 10^{-4}$, which is considered to be sufficiently low to reproduce the behavior of a liquid-liquid system with an infinitely thin (sharp) interface.

Finally, we wish to remind that Jacqmin [22] identified a spatial scale that characterizes the size of a region where diffusion controls the motion of a contact line. In terms of the nondimensional parameters, the nondimensional thickness of the Jacqmin length (that is scaled by the capillary's

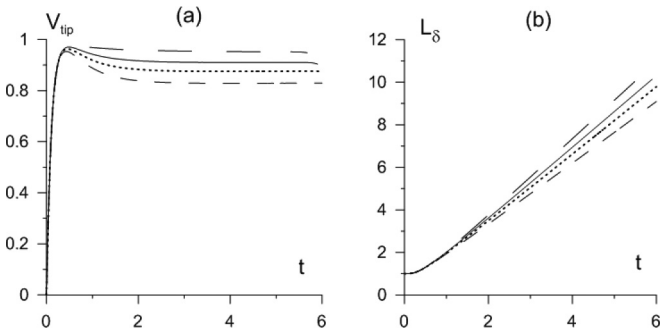

FIG. 2. (a) The velocity of the tip of the liquid-liquid meniscus and (b) the length of the meniscus vs time. The data are obtained for $\mathrm{Pe} = 10^4$, $\mathrm{Re} = 1$, $M = 10^{-2}$ for different Cahn numbers (different interface thicknesses, as $\delta = \sqrt{2\mathrm{Cn}}$) $\mathrm{Cn} = 5 \times 10^{-5}$ (long-dashed lines), $\mathrm{Cn} = 2 \times 10^{-4}$ (solid lines), $\mathrm{Cn} = 4 \times 10^{-4}$ (dotted lines), and $\mathrm{Cn} = 8 \times 10^{-4}$ (dashed lines).

diameter), is $10\sqrt{M/(\mathrm{RePe})} = 10\sqrt{\mathrm{Ca}/\mathrm{Pe}}$. In our work, this length varies from 0.1 (for $M = 1$, $\mathrm{Re} = 1$ and $\mathrm{Pe} = 10^4$) to 10^{-3} (for $M = 10^{-4}$, $\mathrm{Re} = 1$, and $\mathrm{Pe} = 10^4$). This typical length remains greater than the spatial size of the computational mesh, which is also confirmed by the mesh independence of our results.

IV. RESULTS

The numerical problem is characterized by a number of governing parameters. In particular, the behavior of a mixture is strongly affected by the value of the Mach number. Figures 3 and 4 depict the fields of concentration and pressure for three time moments that are obtained for the runs fulfilled for $M = 10^{-2}$ and $M = 10^{-4}$ (or for $\mathrm{Ca} = 10^{-2}$ and $\mathrm{Ca} = 10^{-4}$, as $\mathrm{Re} = 1$). These two cases represent two different scenarios for the motion of the meniscus. In the case of higher Mach number (higher capillary number), the displacement of a liquid from a tube occurs via development of a finger that displaces the liquid from the middle of the tube, although some volume of the liquid remains attached to the tube's walls. The motion of the meniscus's tip occurs considerably faster as compared with the motion of the meniscus's ends, so the interface constantly stretches. One can also notice that the visible (apparent) contact angle that determines the shape of the interface near the wall also constantly changes, becoming smaller. The shape of the interface is determined by the concentration field. Owing to the boundary condition for concentration (10), the isolines of the concentration field always remain orthogonal to the wall, and the contact line also remains orthogonal to the wall. This property can, however, be noticed only if the region near the contact line is magnified.

In the case of smaller Mach number (smaller capillary number), the meniscus propagates down the tube, preserving its shape. The complete displacement of the liquid that initially saturates a tube is observed. One can also notice that at lower values of the Mach number (lower capillary numbers) the speed of the meniscus is considerably lower.

In Fig. 4 one observes that the pressure drops linearly along the tube. Although near the meniscus the pressure isolines become substantially different from a simple set of vertical lines, so the shape of the meniscus could be clearly seen from the isolines of the pressure field. We assume that the fluids stay at rest at the initial moment, when the pressure difference between the tube ends is switched on. Very quickly after that, a "steady" fluid flow is established in a capillary, in terms that the inlet and outlet flow fluxes remain constant; nevertheless, during this motion one liquid is being displaced by another, and the propagation of a liquid-liquid interface induces a nonsteady vortical motion in the tube.

Figure 5 shows the flow fields at an intermediate time moment. In addition to the fields of pressure and concentration, one can also see the field of velocity [Fig. 5(b)]. Far from the meniscus the velocity has a parabolic profile. Near the meniscus the velocity profile is different, and Fig. 5(d) depicts the deviation of the velocity field from the Poiseuille profile (14). One can see that the motion of the meniscus is slowed down by a reverse motion of the fluid near the meniscus's tip. Figure 5(c) also shows the field of chemical potential. Figures 6 and 7 depict the characteristics of the meniscus's motion for the different Mach and Reynolds numbers. The pressure difference that is set between the ends of the tubes (13) is defined to have the maximum velocity equal to 1 when the capillary effects are negligible. The velocity of the meniscus's tip is shown in Fig. 6. The start of the numerical run is characterized by a short adjustment period, during which the flow flux (and the velocity of the meniscus's tip)

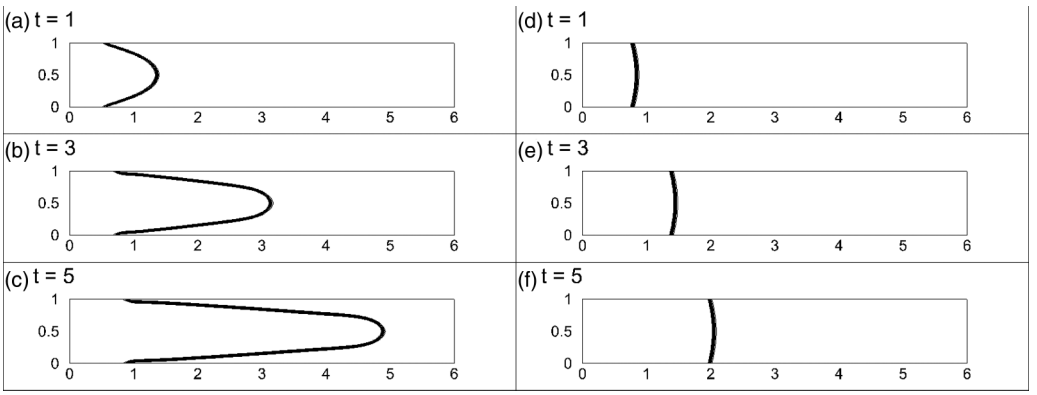

FIG. 3. The typical fields of concentration for different time moments. The data are obtained for $\mathrm{Pe} = 10^4$, $\mathrm{Cn} = 4 \times 10^{-4}$, $\mathrm{Re} = 1$, and two different Mach numbers, $M = 10^{-2}$ (a)–(c) and $M = 10^{-4}$ (d)–(f).

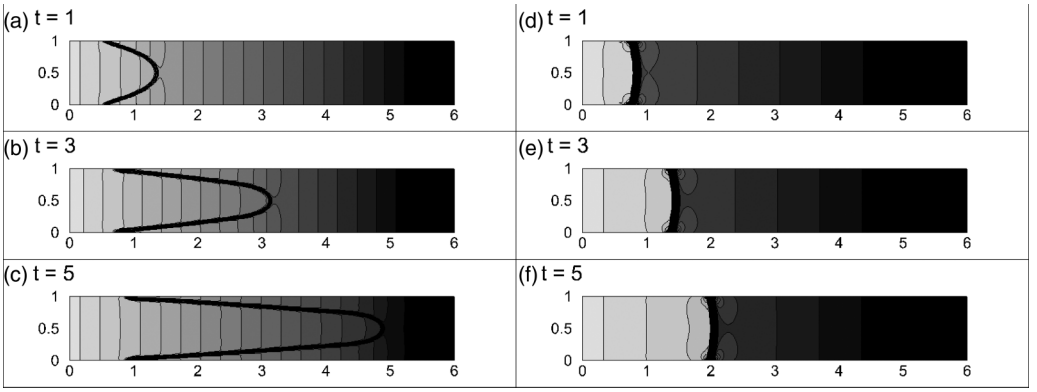

FIG. 4. The typical fields of pressure for different time moments. All parameters as in Fig. 3.

attains a certain constant value, that remains unchanged until the meniscus stays within the tube.

In Fig. 6 one sees that for the higher Mach numbers (or higher capillary numbers), when the surface tension effects are weaker, the velocity profile is just slightly different from the classical Poiseuille profile. For these parameters, the lower the value of the Reynolds number, the closer the velocity of the meniscus's tip (that corresponds to the maximum velocity of the flow) approaches 1, and hence, the closer the flow profile approaches the classical Poiseuille solution (14).

The dependence on the Reynolds number becomes more pronounced at lower Mach numbers. At very low Mach numbers (low capillary numbers), when a pistonlike displacement is observed, the velocity of the meniscus's tip becomes significantly lower than 1, and the dependence on the Reynolds number becomes very weak.

Figure 7 shows the time evolution of the meniscus's length. For higher Mach numbers, the fingering displacement is observed, when the meniscus constantly stretches, and the meniscus's length grows linearly. For very low Mach numbers, the meniscus's length quickly settles to a constant value. The interface stretching depends on the Reynolds numbers and the stretching is minimal at higher Reynolds numbers. Figure 8 shows the velocity profiles at the meniscus's tip and at some distance from the tip (this profile is taken near the outlet, at $x = 5.5$, although the velocity profile remains nearly constant along the tube, except for a very narrow region in the vicinity of the meniscus). One can see that the velocity profile has a parabolic shape, with the maximum value lower than 1. The profile becomes nonparabolic near the meniscus. The greater differences are observed for the case of lower Mach numbers, when the velocity is nearly constant in the bulk (in the region of the meniscus) with two thin boundary layers formed near the tube's walls. The difficulties with resolution of these thin boundary layers explain the slower numerical convergence of the results for lower Mach numbers.

The velocity of the meniscus can be calculated on the basis of the classical Washburn equation [4],

$$V_{\text{tip}} = 1 - \frac{\text{Re}}{8}\left(-\frac{\partial \Pi}{\partial x}\right) = \frac{\text{Re}}{8}\frac{(p_1 - p_2) - p_c}{L} = 1 - \frac{\text{Re}}{8L}p_c. \tag{22}$$

Thus, the flow in a tube is slowed down by capillary forces, and the higher the value of the capillary pressure, the greater the speed of the meniscus's tip differs from 1. Figure 9 depicts the pressure profiles along the centerlines. Outside the meniscus the pressure drops linearly. There is a jump in the pressure levels at two sides of the meniscus, which corresponds to the capillary pressure (the pressure is greater at the concave side of the interface as expected). The capillary pressure depends on the value of the Mach number, which explains the stronger differences of the results obtained for lower Mach numbers (for greater capillary pressures) from the classical Poiseuille flows. It is interesting to note that the capillary pressure that is determined in Fig. 9 and the speed of the meniscus's tip are in favorable agreement with the Washburn equation (22): the capillary pressures in Fig. 9 are approximately 3.2 and 28 for $M = 10^{-2}$ and $M = 10^{-4}$, respectively, which gives the meniscus's velocities, 0.93 and 0.42, and which are close to the values, 0.87 and 0.32, from Fig. 8.

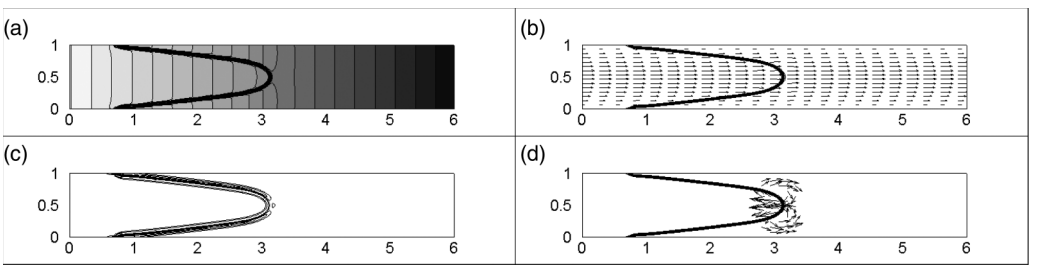

FIG. 5. (a) The fields of pressure (isolines with the density fields); (b) concentration (isolines) and velocity (vectors); (c) chemical potential; and (d) concentration and deviation of the velocity from the Poiseuille profile. The fields are shown for the time moment $t = 3$, and parameters $\text{Pe} = 10^4$, $\text{Re} = 1$, $\text{Cn} = 4 \times 10^{-4}$.

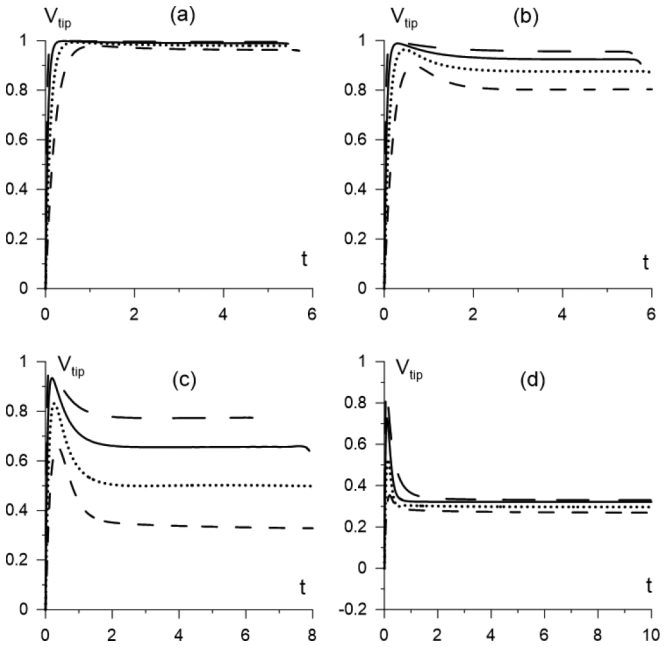

FIG. 6. The velocity of the meniscus's tip for the numerical runs with $M = 10^{-1}$ (a), $M = 10^{-2}$ (b), $M = 10^{-3}$ (c), and $M = 10^{-4}$ (d). The other parameters are $\mathrm{Pe} = 10^4$, $\mathrm{Cn} = 4 \times 10^{-4}$, and different Reynolds numbers, $\mathrm{Re} = 0.25$ (long-dashed lines), $\mathrm{Re} = 0.5$ (solid lines), $\mathrm{Re} = 1$ (dotted lines), and $\mathrm{Re} = 2$ (dashed lines).

The pressure profiles have a sharp peak within the transition zone that separates two liquids. In Fig. 9(b), the peak is cut for a clearer picture. We consider this peak an artefact of the phase-field model. For instance, the phase-field model predicts that the equilibrium concentration profile across the interface is given by the tanh function [14], which is a modeling assumption rather than a real concentration profile.

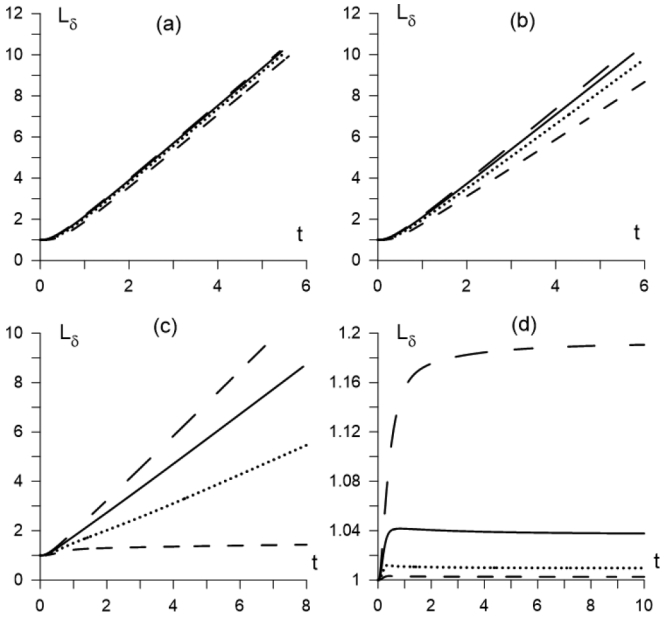

FIG. 7. The time changes of the meniscus's length. The parameters are the same as in Fig. 6.

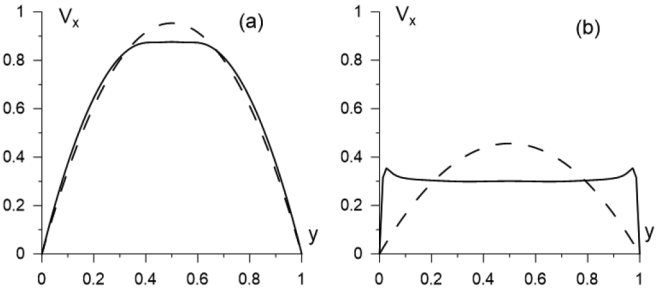

FIG. 8. The profiles of the x component of the velocity across the tube at the points of the meniscus's tip (solid lines) and near the inlet or outlet (dashed lines). The data are obtained for for $t = 3$, $\mathrm{Pe} = 10^4$, $\mathrm{Re} = 1$, $\mathrm{Cn} = 4 \times 10^{-4}$, and two different Mach numbers, $M = 10^{-2}$ (a) and $M = 10^{-4}$ (b).

Similarly, the particular shape of the pressure profile within the liquid-liquid interface is insignificant (and may not be validated by any experimental study), but what is much more important are the levels of the concentration at the sides of the interface, that are measurable, and that are correctly predicted by the phase-field model. The magnitude of this peak depends on the Mach and Cahn numbers. For instance, Fig. 10 depicts the pressure distributions for three values of the Cahn number (or for three different interface thicknesses, as $\delta \sim \sqrt{2\mathrm{Cn}}$). One sees that the magnitude of the peak becomes smaller when the Cahn number (and the interface thickness) tends to zero. This result confirms that the singular behavior in the pressure field is a feature of the numerical approach. The physically correct pressure field that could be obtained in the limit of zero interface thickness would apparently have no peak.

We need to underline that the results in the regions outside of the transitional zone demonstrate the physically relevant behavior even when the value of the capillary number is different from zero (and, also important, that the results in the outer regions are independent of the value of the Cahn number when the Cahn number is sufficiently small). For instance, as earlier demonstrated by Jacqmin [22], the chemical potential within the contact line also exhibits the singular behavior (and that is also observed in our simulations), although "the outer-region velocity field is the same as for sharp interfaces." The surface tension coefficient for the liquid-liquid interface can be calculated from the concentration field using Eq. (19). In Fig. 11 one sees that the surface tension coefficient changes

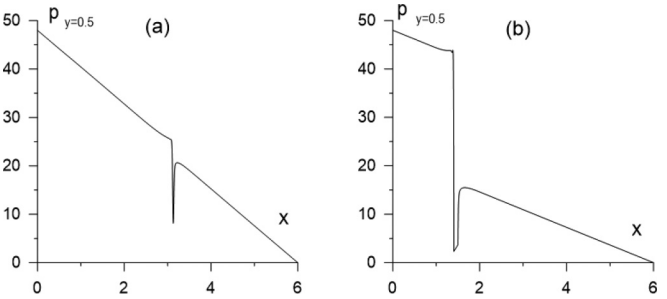

FIG. 9. The profiles of the pressure along the centerline of the tube. The parameters are the same as in Fig. 8.

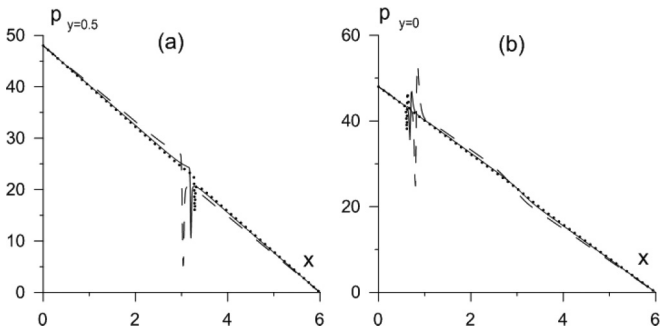

FIG. 10. The pressure profiles along the centerline and along the wall for $M = 0.01$, $\mathrm{Re} = 1$, $\mathrm{Pe} = 10^4$, and three different Cahn numbers, $\mathrm{Cn} = 8 \times 10^4$ (dashed line), $\mathrm{Cn} = 2 \times 10^4$ (solid line), and $\mathrm{Cn} = 5 \times 10^5$ (dotted line). The profiles are shown for $t = 3$.

over time, and these changes are related to interface stretching that alters the interface thickness (and the surface tension coefficient is inversely proportional to the interface thickness) [25]. For lower Mach numbers, when the shape of the meniscus stabilizes, the surface tension coefficient eventually reaches a constant value.

Figure 12 depicts the time changes of the apparent contact angle. For higher Mach numbers, for the fingering displacement, the contact angle becomes smaller and smaller over time, ultimately approaching zero value. If the shape of the meniscus stabilizes then the contact angle takes a certain constant value, which depends on the Mach and Reynolds numbers. For the case of very low Mach numbers and higher Reynolds numbers, the apparent contact angle approaches 90°, which is the static contact angle set by the boundary condition for concentration (10).

For an axisymmetric meniscus enclosed in a capillary, the capillary pressure can be determined using a standard

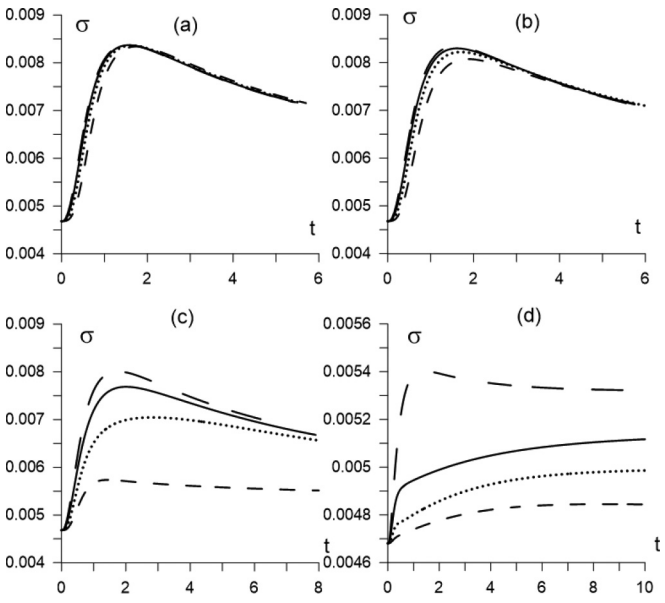

FIG. 11. The time evolution of the surface tension coefficient. The parameters are the same as in Fig. 6.

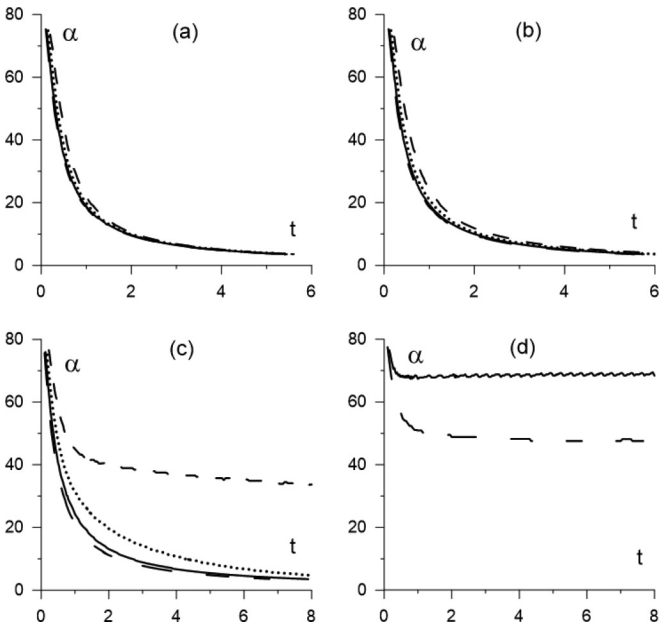

FIG. 12. The time evolution of the dynamic contact angle. The parameters are the same as in Fig. 6. In (d), only two curves are shown for $\mathrm{Re} = 0.25$ and $\mathrm{Re} = 0.5$, as the adopted algorithm for calculations of the contact angle generates too noisy results for higher Reynolds numbers.

equation (written here in the nondimensional form),

$$p_c = \frac{2\sigma \cos(\theta)}{MR}. \tag{23}$$

Here $R = 1/2$ is the capillary's radius.

The values of the capillary pressure that can be determined from Fig. 9 are in a perfect match with the data given by Eq. (23), if one uses the values of the surface tension coefficient and the apparent contact angle from Figs. 11 and 12. For instance, for $M = 10^{-2}$ and $\mathrm{Re} = 1$, the surface tension coefficient equals 0.0079, the apparent contact angle is 7°, and using Eq. (23) one obtains $p_c \sim 3.1$, which is very close to the value 3.2, as in Fig. 9(a). Finally, Fig. 13 depicts the values of the mass fraction of the liquid that initially saturates a capillary and that is eventually left on the capillary's walls. For higher Mach (and capillary) numbers, when the capillary effects are negligible, and the flow profile is close to the Poiseuille flow, $Q = (2/3)V_{\mathrm{tip}}$, and hence $m = 1/3$. This value differs from the asymptotic value $1/2$, reported in numerous studies [6,10,11], which is solely explained by the fact that we consider a 2D geometry, while all other studies deal with 3D configurations. It can be easily shown that for an axisymmetric Poiseuille flow in a tube with the circular cross section, the mass fraction defined by Eq. (20) is $m = 1/2$.

In spite of the difference in the asymptotic values at large capillary numbers, the general dependence predicted by our numerical simulations is in a good agreement with other theoretical and experimental works [6,10,11]. In addition, the calculation of the mass fraction m is traditionally fulfilled for the fingering displacement, although formula (20) may be applied for an arbitrary velocity profile. Figure 13 depicts the data obtained for the fingering and pistonlike displacements, which are marked by the circles and crosses, respectively.

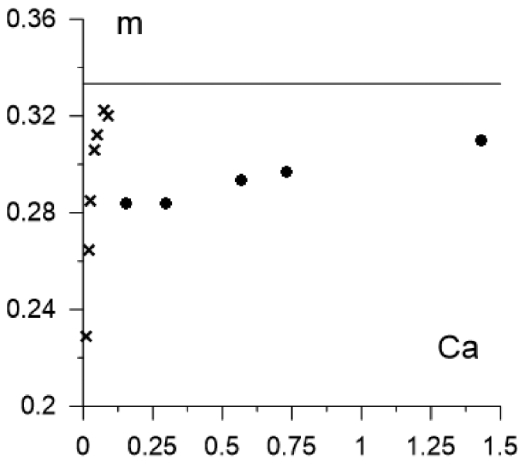

FIG. 13. The mass fraction (20) vs capillary number. The results are shown for $\mathrm{Pe} = 10^4$, $\mathrm{Cn} = 4 \times 10^{-4}$, and different Reynolds numbers. Circles correspond to the fingering displacement, and crosses depict the pistonlike displacements.

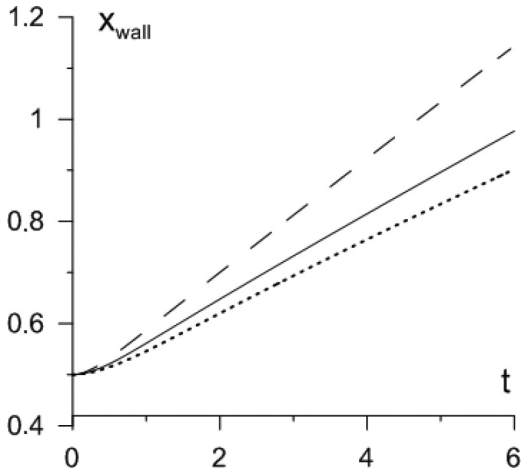

FIG. 15. The position of a meniscus on a wall vs time. The curves are plotted for $M = 10^{-2}$, $\mathrm{Re} = 1$, $\mathrm{Cn} = 4 \times 10^{-4}$ and three different Peclet numbers, $\mathrm{Pe} = 10^3$ (dashed line), $\mathrm{Pe} = 10^4$ (solid line), and $\mathrm{Pe} = 10^5$ (dotted line).

V. DISCUSSION

An apparent difficulty of the direct numerical modeling of the liquid-liquid displacement is the fact that the meniscus may change its shape. The meniscus's shape determines the capillary pressure, and the capillary pressure can alter the flow flux through the capillary. This complex problem seems to be inherently unsteady: even if one agrees that the flow profile from the meniscus is parabolic, the amplitude for this profile remains undefined, as it is determined by the variable capillary pressure. This is a major reason to solve the problem in the formulation of pressure velocity, being able to set the pressure levels at the capillary's inlet or outlet ends, rather then the velocity profiles.

Our results show that the meniscus shape does constantly evolve if the capillary number is sufficiently high (the fingering displacement). The capillary pressure [calculated with the use of Eq. (23)] also experiences some minor changes as can be seen in Fig. 14. Nevertheless, the flow flux through the capillary and the speed of the meniscus remain time independent.

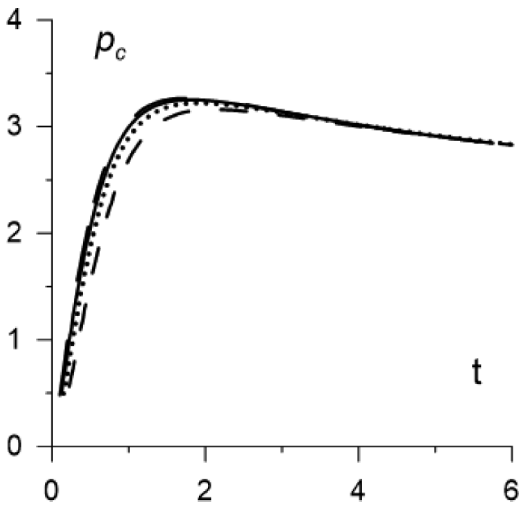

FIG. 14. The capillary pressure as calculated from Eq. (23) vs time. The curves are plotted for $M = 10^{-2}$ and other parameters as in Fig. 6.

Modeling of two-phase flows in a capillary is also complicated by the necessity to reproduce the movement of a contact line. Other researchers either try to avoid this problem by assuming that the wall is completely wetted by one of the liquids [8–10], or adopt the model for the shear-induced slip that introduces an additional phenomenological parameter, the slip length (see, e.g., Ref. [26]).

In the phase-field approach the position of the interface is traced on the basis of the concentration field: movements of an interface, as well as movements of a contact line are explained by the evolution of the concentration field that is determined by the species balance Eq. (3). We need to underline that all flow fields, including the concentration field, are mesh independent in our simulations. The movement of a contact line is ultimately determined by diffusion in a thin region formed near a contact line. The diffusive transport is determined by the Peclet number, and thus this parameter determines the slippage rate of a contact line (see Fig. 15). By performing the simulations for several different Peclet numbers, we show that the flow characteristics depend on this parameter, although no qualitative changes in the flow behavior are observed [for $\mathrm{Pe} = (10^3$–$10^5)$].

VI. CONCLUSIONS

In this work, we provide a direct numerical modeling of the liquid-liquid displacement within the capillary. We consider a wide range of the capillary and Reynolds numbers, reproducing the scenarios of the fingering displacement and the pistonlike displacement of a liquid by injection of another liquid. The phase-field approach is used for modeling the hydrodynamic evolution of two immiscible liquids.

We demonstrate that the phase-field approach is capable of reproducing all features of the liquid-liquid displacement,

predicting the temporal changes of the velocity profile, the interface shape, the capillary pressure associated with the meniscus, the apparent contact angle, and the volume of the liquid that is left on the capillary's walls. In particular, we demonstrate the pressure profiles across the curved meniscus, showing the values of the capillary pressure, which is not available in other studies.

To verify our results, (i) we show that the pressure jump across the interface is well aligned with the value of the capillary pressure that is calculated using the surface tension coefficient that is defined by the integration of the square of the concentration gradient across the interface; and (ii) we show that the effect of the capillary pressure on the motion of fluids through the capillary agrees with the classical Washburn equation. Moreover, far from a fluid-fluid meniscus, the velocity and pressure profiles are also in agreement with classical expectations.

In conclusion, we would like to state that the developed model allows dynamic determination of the capillary pressure and the apparent angle for a liquid-liquid meniscus propagating through a capillary, providing a robust approach for dynamic simulation of the liquid-liquid displacement in a single capillary. In our future work, we aim to adopt this approach for the modeling of the liquid-liquid displacement through a representative element of a porous medium to be given by a regular network of capillaries.

ACKNOWLEDGMENTS

This work was supported by the Russian Foundation for Basic Research (Grant No. 18-01-00782). The numerical calculations were performed using the "Uran" supercomputer of the IMM UB RAS.

[1] E. Aker, K. J. Maloy, A. Hansen, and G. G. Batrouni, Transp. Porous Media **32**, 163 (1998).
[2] M. S. P. Stevar and A. Vorobev, Transp. Porous Media **100**, 407 (2013).
[3] G. D. West, Proc. R. Soc. London, Ser. A **86**, 20 (1911).
[4] E. W. Washburn, Phys. Rev. **17**, 273 (1921).
[5] C. G. Ngan and E. B. Dussan, J. Fluid Mech. **118**, 27 (1982).
[6] G. I. Taylor, J. Fluid Mech. **10**, 161 (1961).
[7] B. G. Cox, J. Fluid Mech. **14**, 81 (1962).
[8] E. J. Soares and R. L. Thompson, J. Fluid Mech. **641**, 63 (2009).
[9] J. F. Freitas, E. J. Soares, and R. L. Thompson, Int. J. Multiphase Flow **37**, 640 (2011).
[10] E. J. Soares, R. L. Thompson, and D. C. Niero, Phys. Fluids **27**, 082105 (2015).
[11] P. Petitjeans and T. Maxworthy, J. Fluid Mech. **326**, 37 (1996).
[12] C.-Y. Chen and E. Meiburg, J. Fluid Mech. **326**, 57 (1996).
[13] J. Cahn and J. Hilliard, J. Chem. Phys. **31**, 688 (1959).
[14] J. Lowengrub and L. Truskinovsky, Proc. R. Soc. London, Ser. A **454**, 2617 (1998).
[15] D. Jacqmin, J. Comput. Phys. **155**, 96 (1999).
[16] H. Ding, P. Spelt, and C. Shu, J. Comput. Phys. **226**, 2078 (2007).
[17] M. Ahmadlouydarab and J. J. Feng, J. Fluid Mech. **746**, 214 (2014).
[18] A. Vorobev, Phys. Rev. E **82**, 056312 (2010).
[19] R. A. Wooding and H. J. Morel-Seytoux, Annu. Rev. Fluid Mech. **8**, 233 (1976).
[20] A. Vorobev, D. Lyubimov, and T. Lyubimova, Phys. Rev. E **95**, 022803 (2017).
[21] L. M. Pismen and A. Nir, Phys. Fluids **25**, 3 (1982).
[22] D. Jacqmin, J. Fluid Mech. **402**, 57 (2000).
[23] J. H. Ferziger and M. Peric, *Computational Methods for Fluid Dynamics* (Springer, New York, 2002).
[24] J. L. Guermond, P. Minev, and J. Shen, Comput. Methods Appl. Mech. Eng. **195**, 5857 (2006).
[25] T. Lyubimova, A. Vorobev, and S. Prokopev, Phys. Fluids **31**, 014104 (2019).
[26] Y. Sui and D. M. Spelt, Phys. Fluids **23**, 122104 (2011).